Computers and Electronics in Agriculture 213 (2023) 108246

Contents lists available at ScienceDirect

Computers and Electronics in Agriculture

journal homepage: www.elsevier.com/locate/compag

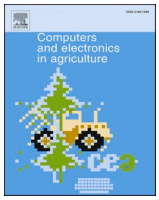

Differentiating nutritional and water statuses in Hass avocado plantations through a temporal analysis of vegetation indices computed from aerial RGB images

Itamar Salazar-Reque [a], Daniel Arteaga [a], Fabiola Mendoza [b], Maria Elena Rojas [b], Jonell Soto [b], Samuel Huaman [a], Guillermo Kemper [a,*]

[a] INICTEL-UNI, Universidad Nacional de Ingeniería, Lima, Peru
[b] Instituto Nacional de Innovación Agraria, Lima, Peru

ARTICLE INFO

Keywords:
Hass avocado
Aerial RGB images
Vegetation Indices
Nutrient Status Monitoring
Water Status Monitoring

ABSTRACT

Maximizing crop production efficiently and sustainably through plant health monitoring is key for global food security. Monitoring large areas with remote sensing technologies such as unmanned aerial vehicles (UAVs) with sensors deals with time and money issues; however, the usage of advanced sensors such as hyperspectral, multispectral and thermal cameras limit their usage among all the stakeholders. In this study we explore different vegetation indices (VIs) extracted from aerial RGB images acquired in different flights to differentiate the nutritional and water statuses of Hass avocado plantations. We used an image processing workflow consisting of image selection through a convolutional neural network (CNN) model, tree crown segmentation, color correction and feature extraction to automate the computation of VIs from RGB images. To compare the performance of VIs in the differentiation of nutritional and water statuses, we proposed a comparison metric called Mean Distance between Vegetation Indices (MDVI), analyzed the evolution of the extracted features, and studied their relationships with gold standard Normalized Difference Vegetation Index (NDVI) measurements. Since the extracted features from each group vary from flight to flight due to multiple factors such as the light intensity of each season and the phenological stage of the plant, the proposed comparison metric leverages the differences between the features extracted from each group, thus reducing these temporal effects. We found that Modified Green Red Vegetation Index (MGRVI) allows a better differentiation of nutritional and water statuses. Furthermore, the correlation coefficients of this VI in the three statuses and NDVI for nitrogen group range between 0.63 and 0.85, indicating a positive strong relationship. The results of this work show that MGRVI has a potential to be used as a correlation variable in studies that only use RGB sensors in order to monitor the nutritional and water status of crops.

1. Introduction

With the current socio-economic and climate change scenarios, ensuring global food security has become a major concern. Projections to 2050 indicate a significant increase in global food demand by 35% to 56% between 2010 and 2050 (van Dijk et al., 2021), placing the onus on the agriculture sector to enhance crop production in an efficient and sustainable manner. Monitoring plant health through nutrient and water status is a viable approach to optimize yields while mitigating environmental impacts. This monitoring provides valuable insights that can be utilized for diagnosing existing nutrient deficiencies, preemptively preventing diseases, and optimizing the use of agrichemicals, fertilizers, and water. By leveraging precision agriculture techniques, farmers can maximize crop production while minimizing costs and environmental impact, thereby ensuring long-term sustainability.

One crop that has garnered considerable attention due to the nutritional and commercial significance, not only of the pulp, but also of the seeds and peel, is the avocado (Persea Americana). For this reason, some studies propose the utilization of seeds and peels (Nyakang'i et al., 2023; Bayomy et al., 2023) based on their abundance of bioactive compounds, including unsaturated fatty acids, vitamins C, B, and E, dietary fiber, lutein, phenolic compounds, as well as various pigments such as

* Corresponding author.
E-mail address: guillermo.kemper@gmail.com (G. Kemper).

https://doi.org/10.1016/j.compag.2023.108246
Received 12 August 2022; Received in revised form 30 August 2023; Accepted 9 September 2023
Available online 22 September 2023

chlorophylls, anthocyanins, and carotenoids (Kosińska et al., 2012; Lu et al., 2005; Saavedra et al., 2017; Wang et al., 2010; Corrales-García et al., 2019; Ong et al., 2022). Consequently, the global production and consumption of avocados have witnessed a substantial surge in recent years. This surge has not only contributed to increased interest in avocado as a functional ingredient in foods but has also led to diverse commercial applications, ranging from frozen products and ice cream to avocado oil, guacamole, and even cosmetic products (Colombo and Papetti, 2019).

Precision agriculture approaches that enable effective monitoring of nutrient and water status, especially in high-value crops like avocados, hold significant promise to cope with the escalating global food demand. Although the advantages provided by precision agriculture, time and money are limitations when monitoring large areas. Current plant analysis in laboratory is not suitable for this scenario because it involves sample collection, sample preparation, laboratory analysis and posterior interpretation. Emerging technologies have been applying to face these limitations. Roper et al. (Roper et al., 2021) discuss some approaches of in vivo plant sensors for plant health monitoring. Remote sensing technologies are also used for the same purpose. UAVs and imaging sensors have been widely employed as a remote sensing system to compute different VIs, which are then used to diagnose nutrient problems (Garza et al., 2020; Janoušek et al., 2021; Noguera et al., 2021) or predict nutrient status (Prado Osco et al., 2019; Zha et al., 2020; Osco et al., 2020).

In most of the studies, the calculation of VIs involves the usage of at least one spectral band other than those of the visible spectrum (the true color bands red, green and blue), such as the near-infrared (NIR) or red edge (RE) bands. This imply the usage of multispectral cameras over UAVs for image acquisition, which can produce a limitation for stakeholders that only possess RGB cameras. To make more extensible the monitoring of nutritional and water status through UAVs and imaging sensors, identifying some VIs extracted from aerial RGB images that are useful for nutritional and water status assessment is required.

This work aims to explore different VIs extracted from aerial RGB images that allow to differentiate trees with adequate and inadequate nutritional and water status. The study was developed with Hass avocado trees. Because of the advantages of fertigation (Incrocci et al., 2017), it was used to induce deficiencies and excesses of nitrogen, phosphorus and potassium (NPK) macronutrients, and water deficiencies. During the study period, a UAV was employed to acquire aerial RGB images of trees with adequate nutritional status (control groups) and trees with an induced inadequate nutritional and water status. Different VIs were calculated for each group and flight, which then were used to compute the comparison features. We proposed a comparison metric called Mean Distance between Vegetation Indices (MDVI) that allows better differentiation among statuses for different groups and VIs. In addition, a temporal analysis of these features and a correlation study with NDVI (Rouse et al., 1974) measurements were performed. Our results show that MGRVI (Bendig et al., 2015) performed better in differentiating nutritional and water statuses.

Therefore, in this study, we propose a novel approach to differentiate the nutritional and water statuses in Hass avocado plantations through a temporal analysis of VIs computed from aerial RGB images. By employing remote sensing techniques and advanced image analysis algorithms, we aim to develop a non-invasive and cost-effective method for assessing the nutrient and water status of Hass avocado trees. Such an approach has the potential to empower farmers with valuable information to make informed decisions regarding nutrient and water management, leading to improved yields and sustainable avocado production.

2. Related work

One of the main limitations for the increase in crop productivity is the availability of water and nutrients like nitrogen. Macronutrients intake for plants is closely related with the amount of water in the soil; therefore, during drought, crops are negatively affected due to water and nitrogen constraints (Plett et al., 2020). In order to determine and control the nutrients and water in plants, different monitoring procedures have been employed.

Silber et al. (2018) assessed the seasonal nutritional requirement of Hass avocado trees grown in lysimeters. Through this in-situ monitoring of NPK macronutrients, they determined that continuous nutrient application during the year, and the modification of fertilization rate together with the nutrient combination is required for guaranteeing optimal yield. Moreover, they conclude that fruit analyses should be used for scheduling fertilization instead of leaf analyses. Gaona et al. (2020) also employed an in-situ monitoring procedure to determine the effect of two doses of nitrogen and potassium in the initial growth phase of Hass avocado. They observed significant differences in the greenery index and nutrient concentration variables.

In-situ monitoring allows accurate evaluation of the nutritional and water status of plants; nevertheless, it is time consuming and normally requires the completion of specific steps to interpret the data (Dezordi et al., 2016). Remote sensing technologies cope with this drawback. Monitoring of the nutritional and water status with remote sensing systems allows to cover medium and large areas in less time and data processing is done autonomously through computer programs.

Satellites are very popular remote sensing monitoring systems that have been used for many precise agriculture applications such as pesticide usage monitoring (Adan et al., 2021), pest severity assessment (Salgadoe et al., 2018), yield mapping (Robson et al., 2017), and nutritional plant status monitoring (Sharifi, 2020; Sims et al., 2013). Sims et al. (2013) presented a synopsis of studies using satellite hyperspectral imagery for foliar nutrition assessment which collectively demonstrate that several important nutrients can be accurately mapped at critical ages for the management of plantation forests. However, some spatial and radiometric characteristics limit the practical usage. Sharifi (2020) used satellite imagery to evaluate the use of VIs for crop nutrition mapping. They found that the two best VIs were TCARI (Transformed Chlorophyll Absorption in Reflectance Index) (Haboudane et al., 2002) and MCARI (Modified Chlorophyll Absorption in Reflectance Index) (Daughtry et al., 2000). Moreover, they conclude that the use of NIR and RE multispectral bands in mid-season led to better results than VIs calculated at the end of the season or that do not include the RE band.

With the development of UAVs and imagery sensors in the recent years, there are more studies in the monitoring of nutritional and water status of plants. A review article by Jayme Arnal (Barbedo, 2019) presented 30 and 31 works dealing with the monitoring of nutrient and water status in crops respectively. On one hand, multispectral cameras were the sensors used in most of the studies for monitoring of nutritional status. On the other hand, most of the studies aiming to monitor water status employed thermal cameras.

Regarding the studies with multispectral images, Lu et al. (2019) acquire images at seven view zenith angles for three critical growth stages of winter wheat and computed four VIs as input variables: Visible Atmospherically Resistant Index (VARI) (Gitelson et al., 2002), Red edge Chlorophyll Index (CIred-edge) (Gitelson et al., 2003; Gitelson, 2005; Gitelson et al., 2006), Green band Chlorophyll Index (CIgreen) (Gitelson et al., 2003; Gitelson, 2005; Gitelson et al., 2006), and Modified Normalized Difference Vegetation Index with a blue band (mNDblue) (Jay et al., 2017). They used leaf nitrogen concentration (LNC), plant nitrogen concentration (PNC), leaf nitrogen accumulation (LNA), and plant nitrogen accumulation (PNA) as target variables to be estimated by a linear regression model. When using multiple view zenith angles, they used a two-variable regression model. The best result with single-angle images was obtained with CIgreen for LNC from a view zenith angle of -60°. Zhang et al. (2016) monitored heading rice growing based on UAV multispectral images by using linear regression model. They used GNDVI (Green Normalized Difference Vegetation Index) (Buschmann and Nagel, 1993) as input variable, and SPAD values (chlorophyll) and

the nitrogen content as target variables, finding a higher correlation between GNDVI and SPAD values. Another usage of multispectral images to compute VIs for estimating nutritional status was presented by Chungcharoen et al. (2022). In this study, they computed 34 VIs and 10 features based on average and standard deviation values to be used as input variables for analyses against 10 target nutritional status variables (encompassing NPK). They employed four machine learning techniques (Random Forest, Support Vector Regression, Partial Least Square Regression, and Artificial Neural Network) finding that models for chlorophyll, nitrogen and calcium predictions were acceptable for screening. The screening model based on Support Vector Regression for nitrogen obtain a coefficient of determination ranging from 0.665 to 0.718. Similarly, Guerra-Hernández et al. (2021) acquired multispectral images with a UAV to monitor health status in priority riparian forest. They considered 34 remote sensing variables such as VIs, texture features from NDVI and digital surface model, among others. The objective was to classify trees in four categories: asymptomatic, dead, and defoliation above and below 50% threshold. The classification using Random Forest with four, three (asymptomatic, defoliated, dead) and two (alive, dead) classes yielded overall accuracies of 0.67, 0.72 and 0.91 respectively. By using three logistic models with leave-out cross validation method the accuracies were 0.75, 0.8 and 0.94 respectively.

RGB images acquired via UAVs have been also used in monitoring plant health – nutrient and water – status. Garza et al. (2020) correlates the triangular greenness index (TGI) (Hunt et al., 2011) with field measurements such as mineral nutrients and foot rot disease severity to distinguish trees with disease. They found that TGI was different depending on disease or in combination of diseases and also explained which factors were involved in these differences. Qiu et al. (Qiu et al., 2021) calculated different VIs from RGB images acquired through a UAV and showed they are correlated with nitrogen nutrition index (NNI) for rice at different growth stages. Ballesteros et al. (2018) estimated crop biomass (which involves pest and weed status, soil quality, water stress, yield prediction, among others) from high-resolution RGB images obtained with a UAV. They extracted green canopy cover, crop height and canopy volume for predictor variables, finding strong correlation between canopy volume and dry leaf biomass and dry bulb biomass. A method for monitoring health status of Eucalyptus pellita in a large-scale area through the usage of RGB images acquired with a UAV was proposed by Megat Mohamed Nazir et al., (2021). They generated an *ortho*-image and computed VARI-green (Gitelson et al., 2002) to classify four levels of pest and disease: dead, severely infected, mildly infected and

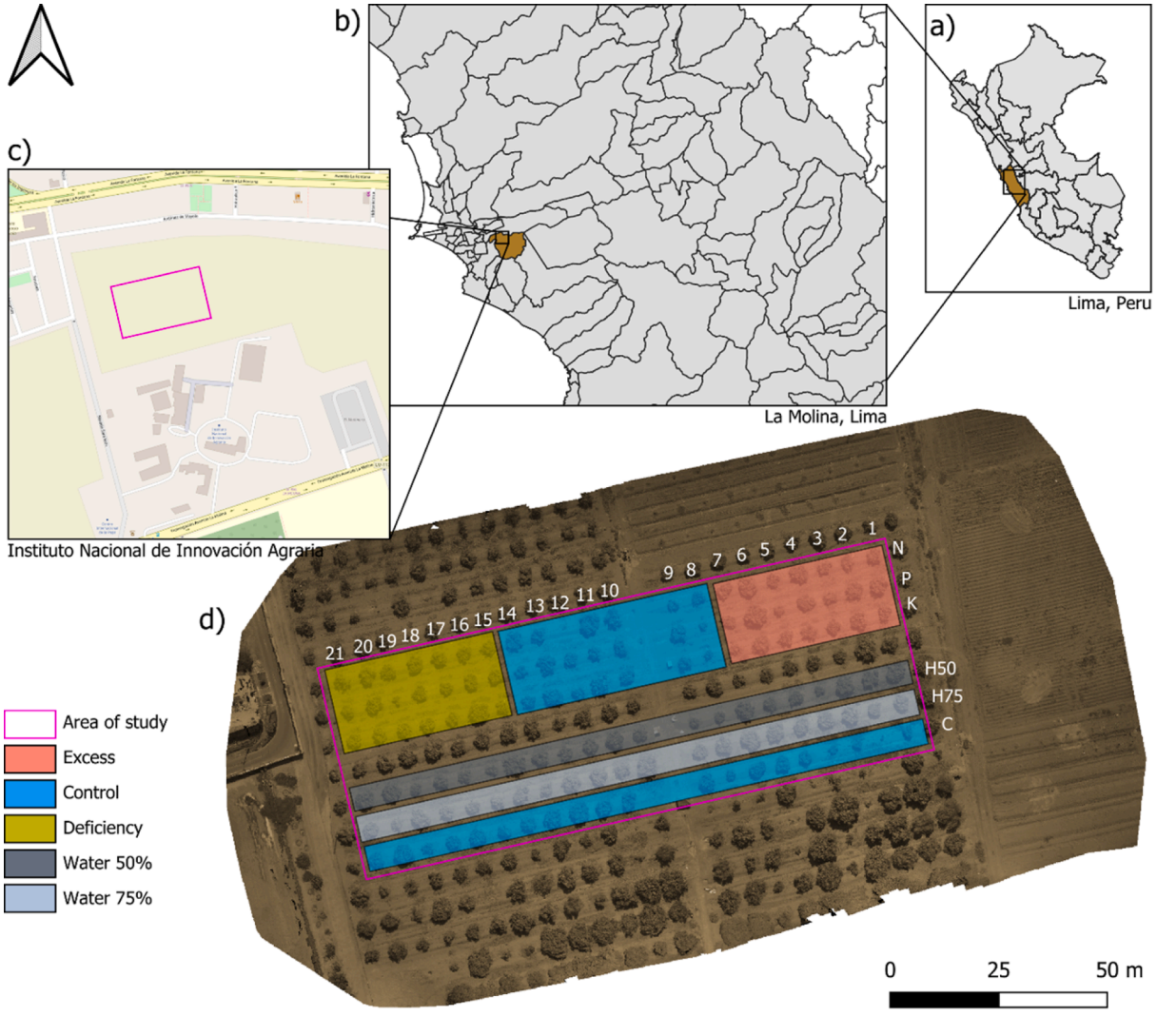

Fig. 1. Geographic location from the study area. a) Lima location (brown colored) related to Peru. b) La Molina location (brown colored) related to Lima. c) National Institute of Agrarian Innovation (INIA) and study area (pink box). d) Mosaicked image from study area in false color. Fill-colored rectangles group trees with some common features. (For interpretation of the references to color in this figure legend, the reader is referred to the web version of this article.)

healthy trees. The VARI-green indices were verified by manual ground-true values and by comparison with NDVI, showing a correlation of 0.73. Ge et al. (2021) estimated PNC of rice using a fusion of VIs and color moments from UAV-based RGB images. They used Partial Least Square Regression and Random Forest models and demonstrated that the fusion of VIs and color moments as input variables improve the accuracy of PNC estimation compared to VIs or color moments only.

3. Methodology

3.1. Area of study

This study was conducted over a hectare of Hass Avocado at the National Institute of Agrarian Innovation located (INIA) in La Molina, Lima, Peru (see Fig. 1a-c). We analyzed 123 trees that were distributed in seven rows and twenty-one columns (pink box in Fig. 1d). The separation between trees was five meters approximately as show in Fig. 2. Latitude and longitude coordinates from study area vertices are: (−12.074588, −76.947483), (−12.074266, −76.946131), (−12.074826, −76.946021) and (−12.075139, −76.947359). Trees were six meter tall and three years old on average. The soil was loan with an average pH of 7.55 and an electrical conductivity of 2.06 $mS\,cm^{-1}$ (measured according to UNE 77308:2001 using a mixture of soil and water in the ratio 2 to 1). The organic matter value was 0.55. Soil phosphorus (P) and potassium (K) values were 18.7 ppm and 355 ppm respectively. These values were obtained from a laboratory analysis of soil samples at different layers made in January 2020.

3.2. Experimental design

3.2.1. Macronutrient variation experiment

The first three rows in the study area were used to study the effect of different levels of macronutrients, either nitrogen (N), phosphorus (P) or potassium (K) in the trees. We provided nutrients using fertigation as it allowed us to vary the amount of macronutrients in a practical way. We varied the level of one macronutrient while keeping the others and water in optimal conditions. Trees in each row were subdivided in three statuses according to the level of the nutrient: excess (red), control (blue sky) and deficiency (yellow) (see Fig. 1d). For example, a tree located in N-7 has excess of nitrogen; P-19 has deficiency of phosphorus and K-12 is control of potassium (i.e., potassium in optimal conditions). To induce these statuses, macronutrients were provided in the amounts shown in Table 1 in three different dates: May 10th, September 6th and November 15th.

3.2.2. Water variation experiment

The last three rows in the study area were used to study the effect of different levels of water in the trees. We varied the level of water while keeping macronutrients in optimal conditions. Each row had a different level of water: 50% (black), 75% (gray) and control (sky blue) (see Fig. 1d and Table 1). Water pressure through the pipes was controlled to induce the three different water statuses.

3.3. NDVI measurements

Normalized Difference Vegetation Index (NDVI) has been used widely in the literature to analyze crops. We captured in-field NDVI measurements using the GreenSeeker Handheld Crop Sensor. Measurements were taken approximately 60 cm above the top of the tree with the help of a step ladder.

Table 1
Amount of macronutrients and water provided to trees per group and statuses.

Group (G)	Status (s)	N	P	K	Water
N	Excess	120 $kg\,ha^{-1}$	60 $kg\,ha^{-1}$	80 $kg\,ha^{-1}$	100%
	Control	80 $kg\,ha^{-1}$	60 $kg\,ha^{-1}$	80 $kg\,ha^{-1}$	100%
	Deficiency	0 $kg\,ha^{-1}$	60 $kg\,ha^{-1}$	60 $kg\,ha^{-1}$	100%
P	Excess	80 $kg\,ha^{-1}$	100 $kg\,ha^{-1}$	80 $kg\,ha^{-1}$	100%
	Control	80 $kg\,ha^{-1}$	60 $kg\,ha^{-1}$	80 $kg\,ha^{-1}$	100%
	Deficiency	80 $kg\,ha^{-1}$	0 $kg\,ha^{-1}$	60 $kg\,ha^{-1}$	100%
K	Excess	80 $kg\,ha^{-1}$	60 $kg\,ha^{-1}$	120 $kg\,ha^{-1}$	100%
	Control	80 $kg\,ha^{-1}$	60 $kg\,ha^{-1}$	80 $kg\,ha^{-1}$	100%
	Deficiency	80 $kg\,ha^{-1}$	60 $kg\,ha^{-1}$	0 $kg\,ha^{-1}$	100%
Water	Control	80 $kg\,ha^{-1}$	60 $kg\,ha^{-1}$	80 $kg\,ha^{-1}$	100%
	75	80 $kg\,ha^{-1}$	60 $kg\,ha^{-1}$	80 $kg\,ha^{-1}$	75%
	50	80 $kg\,ha^{-1}$	60 $kg\,ha^{-1}$	80 $kg\,ha^{-1}$	50%

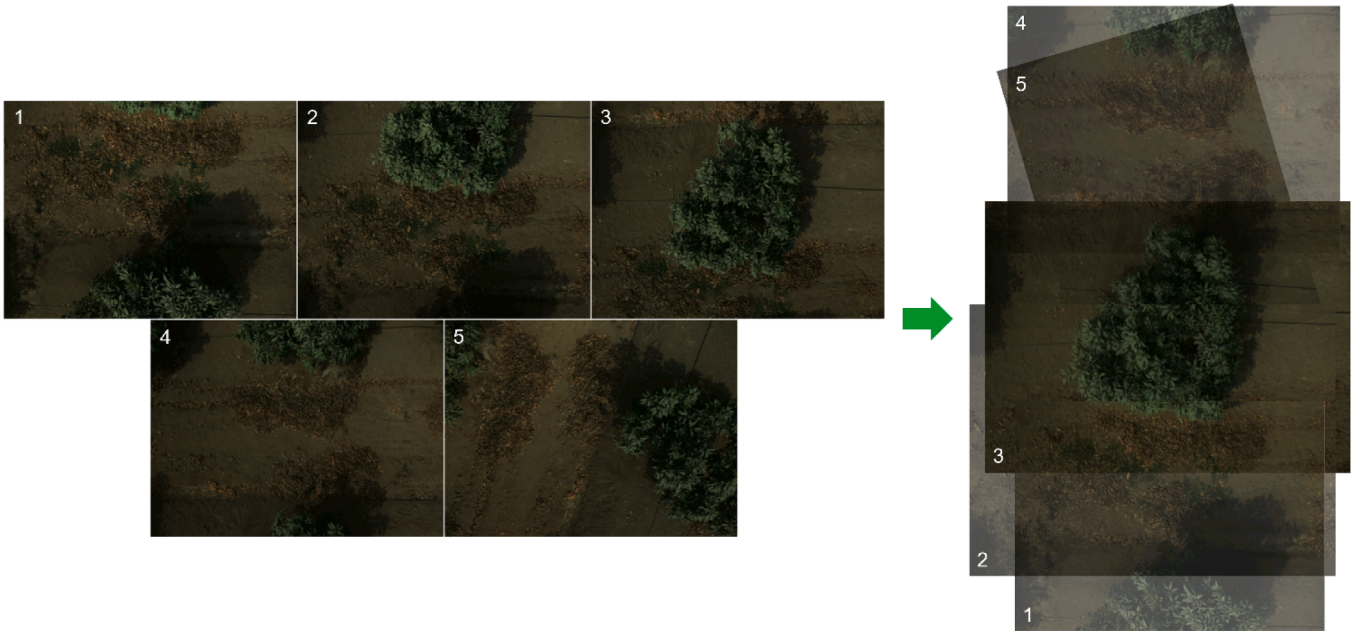

Fig. 2. Sequential images acquired from a single tree using UAV. Note that before any image processing we need to select the best acquired image (number 3 in this case).

3.4. Image acquisition

Images from the top of the trees were acquired using a Phantom Pro V2 UAV from DJI (https://www.dji.com/phantom-4-pro-v2) equipped with a SENTERA Double 4 K multispectral camera. This camera has two lenses: one of them acquires RGB images and the other, NIR and RE bands together. In this study we are interested in the use of RGB images.

The UAV flights followed a single grid path starting in tree N-1 and finishing in tree C-21 as shown in Fig. 1d. To do so, coordinates of each row extreme were set in the flight planning software considering a height of 7 m above the ground. UAV was configured to have an average speed of 2 m/s and images were acquired every 1 s. Although, this configuration implies to have more images than trees, we guarantee to complete the desired path rapidly and to have at least one image of a complete tree with the least number of images per flight. A sample of continuous images acquired under this configuration is shown in Fig. 2, note that as there are many images per tree we will need to select the best. The procedure to deal with image selection is described in section 3.5.

We conducted 21 flights over a period of seven months. Each flight acquired an average of 700 georeferenced images (some of them will be discarded). Dates, number of images as well as some flight conditions are reported in Table 2.

3.5. Image processing

For each flight we have to follow a procedure composed of three steps in order to generate a proper feature to compare between statuses.

Table 2
UAV flights information.

Date	DOY (t)	# of images	Flight conditions
March 29	88	835	RH: 56, T: 24, WS: 2
April 14	104	820	RH: 67, T: 22, WS: 3, LCC: 6, MCC: 0, HCC: 82
April 28	118	760	T: 27, WS: 2.5, LCC: 1, MCC: 1, HCC: 41
May 7	127	702	T: 25.5, WS: 3, LCC: 3, MCC: 13, HCC: 0
May 12	132	805	T: 24, WS: 2, LCC: 13, MCC: 5, HCC: 20
May 19	139	730	RH: 81, T: 23.5, WS: 3, LCC: 0, MCC: 0, HCC: 0
May 26	146	750	RH: 78.5, T: 24, WS: 1, LCC: 13, MCC: 8, HCC: 0
Jun 02	153	835	WS: 2, LCC: 59, MCC: 0, HCC: 7
Jun 11	162	820	RH: 62, T: 19, WS: 3, LCC: 17, MCC: 3, HCC: 0
Jun 16	167	795	RH: 73, T: 27, WS: 3, LCC: 2, MCC: 0, HCC: 2
Jun 23	174	889	T: 18, WS: 3, LCC: 12, MCC: 0, HCC: 19
July 02	183	803	RH: 54, T: 19.5, WS: 2, LCC: 43, MCC: 0, HCC: 1
July 09	190	786	RH: 53, T: 22, WS: 2, LCC: 4, MCC: 0, HCC: 0
July 14	195	708	–
July 23	204	750	RH: 62, T: 20, WS: 3, LCC: 21, MCC: 0, HCC: 0
August 05	217	770	RH: 76, T: 20.5, WS: 3, LCC: 55, MCC: 0, HCC: 0
August 13	225	802	RH: 60, T: 20.5, WS: 3, LCC: 5, MCC: 1, HCC: 10
August 19	231	815	–
September 15	258	752	RH: 60, T: 19, WS: 3, LCC: 5, MCC: 1, HCC: 2
September 24	267	798	RH: 62, T: 21, WS: 2, LCC: 10, MCC: 0, HCC: 6
October 15	288	770	–
October 24	302	821	RH: 62, T: 23, WS: 2, LCC: 62, MCC: 4, HCC: 4

Note: RH: relative humidity, T: ambient temperature in Celsius degrees, WS: wind speed, LCC: percentage of low cloud cover, MCC: percentage of medium cloud cover, HCC: percentage of high cloud cover.

First, we have to clean our image set per flight and tag them according to the group and status they belong to by performing image selection through a CNN. Next, we need to perform a proper crown segmentation of the trees. Finally, leveraging these segmentations several features per group, status and flight are extracted for comparison. These steps were performed through Python scripts. A summary of this procedure is shown in Fig. 3.

3.5.1. Image selection based on CNN

As mentioned before, our flight configuration allowed us to complete the acquisition in a few minutes but with the compromise of having unnecessary images (see Fig. 2). Thus, we need to clean our image set and tag each image according to the group and status the tree belongs to. To do so, we perform the following steps which are based on our previous work on tree image selection (Salazar-Reque et al., 2021):

A manual selection of "best images" per tree was made for one flight. This is done only once and will be used as a reference in future flights. Manual selection means human selection and "best images" stand for those images in which all or the most of the tree crown appears, and in which it is as centered as possible.
An automatic pre-selection of images per tree was made based on proximity using geolocation information from images from step 1.
We generate binary masks per each image from step 2 using a UNET (Ronneberger et al., 2015) like architecture trained for coarse crown segmentation of trees.
Binary images from step 3 were used to discard images that do not meet the criteria of a good acquisition (e.g., tree centered in the image).
We select the best image available per tree by comparing binary masks from images from step 4 with binary masks from the images of reference from step 1. As each tree is associated with a group, the

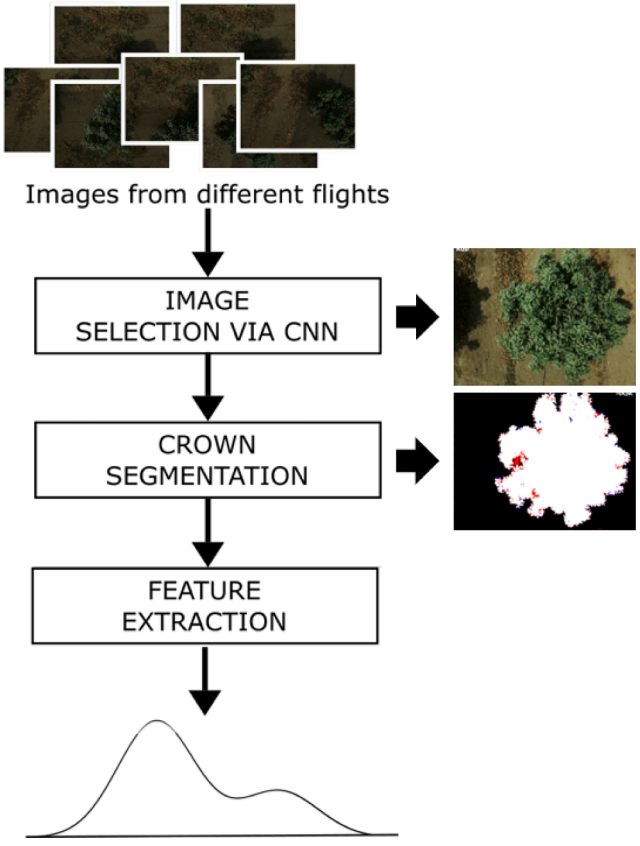

Fig. 3. Image processing flowchart.

final outcome is one image per tree labeled according to their corresponding group.

If we repeat this process in every flight, we ended up with a set of images ordered by tree and date.

3.5.2. Crown segmentation

Previous binary masks were coarse crown segmentations that were useful for tree image comparison with reference images from another flight. However, when viewed in detail, these binary masks also include shadows or poorly lit areas of the trees that can generate artifacts in the features we are intended to generate. To reduce these artifacts, we eliminate these dark areas by means of the Otsu's method (Otsu, 1979) on each of the color components of the RGB images clipped to the rectangle with the maximum area that is inside the segmented tree. Otsu's method maximizes the means and minimizes the variance of the distribution of pixel values by assuming that there are two groups (leaves and dark areas in our case). Thus, we reduce the influence of dark areas in the final features.

3.5.3. Feature extraction

Using our previous crown segmentations, we can create a set of N_p square patches per group G in a given time t. Then, for each of these patches we compute its density function $h_G^{(i)}(x;t)$ for a random variable X where $i = 1,\ldots,N_p$. Our objective here is to generate a signal $z_G(t)$ that represents the temporal evolution of group G. We compute this signal as the expected value over X as follows:

$$z_G(t) = \mathbb{E}[f_G(x;t)] \tag{1}$$

where $f_G(x;t)$ represents the probability density function of a group G in a given time t. This is computed as the average of the previous density functions $h_G^{(i)}(x;t)$.

$$f_G(x;t) = \frac{1}{N_p}\sum_{i=1}^{N_p} h_G^{(i)}(x;t) \tag{2}$$

The random variable X is defined by the pixel-wise combination between red, green and blue channels according to the VI of interest. The VIs explored in this work are the same used in (Qiu et al., 2021) which we summarized in Table 3.

Table 3
Vegetation indexes explored.

Vegetation Index	X	References
Red Green Ratio Index (RGRI)	r/g	(Gamon and Surfus, 1999)
Blue Green Ratio Index (BGRI)	b/g	(Yue et al., 2018)
Green Leaf Algorithm (GLA)	$(2g-r-b)/(2g+r+b)$	(Louhaichi et al., 2001)
Green Leaf Index (GLI)	$(2g-r+b)/(2g+r+b)$	(Qiu et al., 2021)
Green Red Vegetation Index (GRVI)	$(g-r)/(g+r)$	(Tucker, 1979)
Modified Green Red Vegetation Index (MGRVI)	$(g^2-r^2)/(g^2+r^2)$	(Bendig et al., 2015)
Excess Green minus Excess Red (ExGR)	$(2g-r-b)-(1.4r-g)$	(Meyer and Neto, 2008)
Excess Red Vegetation Index (ExR)	$1.4r-g$	(Meyer et al., 1998)
Excess Blue Vegetation Index (ExB)	$1.4b-g$	(Mao et al., 2003)
Excess Green Vegetation Index (ExG)	$2g-r-b$	(Woebbecke et al., 1995)
Visible Atmospherically Resistant Index (VARI) []	$(g-r)/(g+r+b)$	(Gitelson et al., 2002)
Red Green Blue Vegetation Index (RGBVI)	$(g^2-br^2)/(g^2+br^2)$	(Bendig et al., 2015)

Note: All operations are pixel-wise operations.

3.6. Comparison metric

To compare the differentiation between nutritional and water statuses that each VI indicates, we proposed the Mean Distance between Vegetation Indices (MDVI) as a metric (see Equation 3).

$$MDVI_{VI}(s_1,s_2) = \frac{1}{T}\sum_t |z_{s_1}(t) - z_{s_2}(t)| \tag{3}$$

In Equation 3, $z(t)$ is the value of *VI* at time *t*. The value of *VI* at time *t* for a certain status *s* is denoted as $z_s(t)$, so the distance between VIs for statuses s_1 and s_2 at time *t* is the absolute value of the difference between $z_{s_1}(t)$ and $z_{s_2}(t)$. Finally, to compute the mean value of this distance, the absolute value of the difference ($|z_{s_1}(t) - z_{s_2}(t)|$) for each time *t* is summed together and divided by the total number of time instants *T*. This allows comparisons between studies with different temporal resolutions. MDVI basically computes the area of the difference between the temporal evolution (signals) of VIs for the compared statuses per time instant, and therefore this is a measurement of how similar or different the temporal evolution of VIs for each status are.

4. Results

4.1. Comparison of VIs

Taking into consideration the groups, denoted by *G*, Equation 3 can be formulated as follow:

$$MDVI_{VI}^{G}(s_1,s_2) = \frac{1}{T}\sum_t |z_{s_1}^{G}(t) - z_{s_2}^{G}(t)| \tag{3}$$

For each VI in Table 3, we computed a value of $MDVI_{VI}^{G}(s_1,s_2)$ where *G* represented the group and was either {N, P, K or W} and s_1 and s_2 represented the statuses and were chosen from {Excess, Control or Deficiency} for macronutrients or from {50, 75 or Control} for water (W). This computation also involves to calculate $z_s^G(t)$ for each DOY (see Table 2). It is important to mention that MDVI computation for a group involves multiple trees, so $z_s^G(t)$ is the average value of *VI* for all the trees belonging to group *G* at time *t* for a certain status *s*.

The MDVI values for each combination of groups, statuses and VIs are summarized in the plots shown in Figs. 4 and 5. Better differentiation between statuses is achieved for nitrogen because most MDVI values are higher for this group ($MDVI_{VI}^{N} > MDVI_{VI}^{P}$ and $MDVI_{VI}^{N} > MDVI_{VI}^{K}$) as shown by red lines being in the outermost part of the radar plot compared to blue and green lines. Similar MDVI values (but usually lower than nitrogen) were obtained in the phosphorus group. For potassium, the MDVI values for any VIs were always lower than for nitrogen and phosphorus. In general, this shows that it is harder to distinguish between groups for this macronutrient, especially when a deficiency status is involved.

When analyzing only the results for nitrogen and phosphorus groups, we note that higher values of MDVI were always given by MGRVI. This indicates that this VI better differentiates between statuses for these macronutrients. Not surprisingly, the Excess vs Deficiency statuses comparison was easy to differentiate than the others as can be noted by the higher MDVI values reported. On the other hand, the Deficiency and Control statuses comparison had the smallest values indicating that lack of nitrogen or phosphorus macronutrients are difficult to distinguish from controls.

A similar analysis can be done for the water experiment results. Again, MGRVI has the higher values of MDVI (see Figs. 4 and 5) but only for 50% vs CONTROL and 50% vs 75% comparisons. In the case of of 75% vs CONTROL comparison we can expect that these statuses to behave very similar as MDVI values for this comparison are very low for all the VIs.

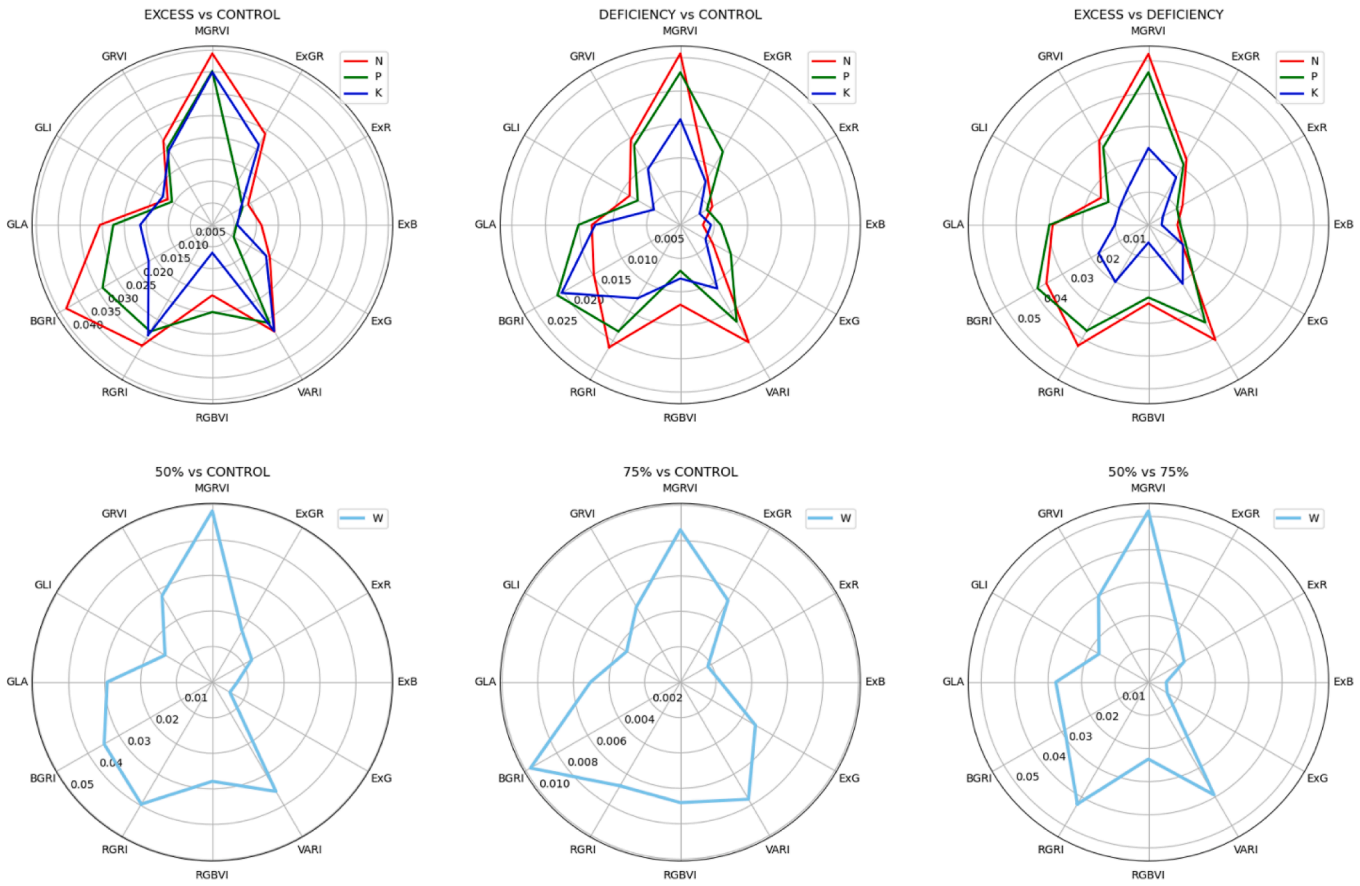

Fig. 4. MDVI values for each combination of groups, statuses and VIs. First row: Comparison between excess and control statuses (left), comparison between deficiency and control statuses (middle) and comparison between excess and deficiency statuses (right). Second row: Comparison between water50 and control statuses (left), comparison between water75 and control statuses (middle) and comparison between water50 and water75 statuses (right).

Fig. 5. Bar plots with MDVI values for multiple VIs. Each row represents a group, and each column represents a pair of statuses being compared.

4.2. Temporal analysis of VIs for nitrogen group

As the MDVI values were higher for nitrogen group, we decided to analyze the temporal evolution of NDVI compared with three VIs that allow good (MGRVI), normal (GLA) and poor (ExB) differentiation (according to MDVI) for this group (see Fig. 6). This selection is due to we wanted to perform a posterior correlation study with NDVI, so the possibility of unexpected correlations had to be considered. For the computation of the distributions, we have used 50 bins in the range of [-0.2, 0.8]. We used this range because VIs varied between those values. NDVI values were computed from multispectral images acquired in the same flight conditions with a Sentera Double 4 K Sensor Multispectral camera (https://sentera.com/products/fieldcapture/sensors/double-4k/).

4.3. Correlation with NDVI measurements

The results of correlation study (see Table 4) demonstrate a positive relationship between MGRVI for nitrogen group and NDVI due to the correlation coefficients in the three statuses range from 0.63 to 0.85. These values were computed considering the fruit and harvesting period (approximately from DOY 163 to DOY 259).

5. Discussion

The purpose of this study was to investigate the relationship between NPK macronutrients status and VIs as well as water status and VIs. In this discussion, we will compare our results with findings from other authors, providing a more comprehensive analysis of the obtained results and their implications. Our findings regarding macronutrient status and VIs align with previous studies in the field. Nitrogen has demonstrated the highest differentiating power among the macronutrients analyzed, which is consistent with the strongest influence this macronutrient has on tree growth and development as reported by Jiaying et al. (2022) and Silber et al. (2022).

Table 4
Correlation between NDVI and RGB-based vegetation indices for different nitrogen statuses.

VI	Deficiency	Control	Excess
GLA	0.6585	0.7921	0.4775
MGRVI	**0.8086**	**0.8488**	**0.6289**
ExB	−0.2863	−0.4269	−0.2909

In Figs. 4 and 5, we presented radar and bar plots that demonstrate the differentiation between macronutrient statuses based on MDVI values for each VI. Notably, MGRVI, BGRI, RGRI, and VARI consistently outperformed other indices in differentiating between the nitrogen and phosphorus groups, particularly for nitrogen. These findings are consistent with the results reported in previous studies (Qiu et al., 2021; Megat Mohamed Nazir et al., 2021).

Interestingly, the worst-performing indices (ExB, ExR, and ExG) were those computed using linear operations of color components, while best VIs always involved a non-linear operation (a division). This might be due to the fact that images acquired by UAV are prone to light variations and division between color components are more robust to this kind of artifacts than linear combination, as discussed by (Barbedo, 2017) in the context of disease segmentation over leaves.

As anticipated, the MDVI values were highest when comparing the excess and deficiency groups, demonstrating their strong discriminatory

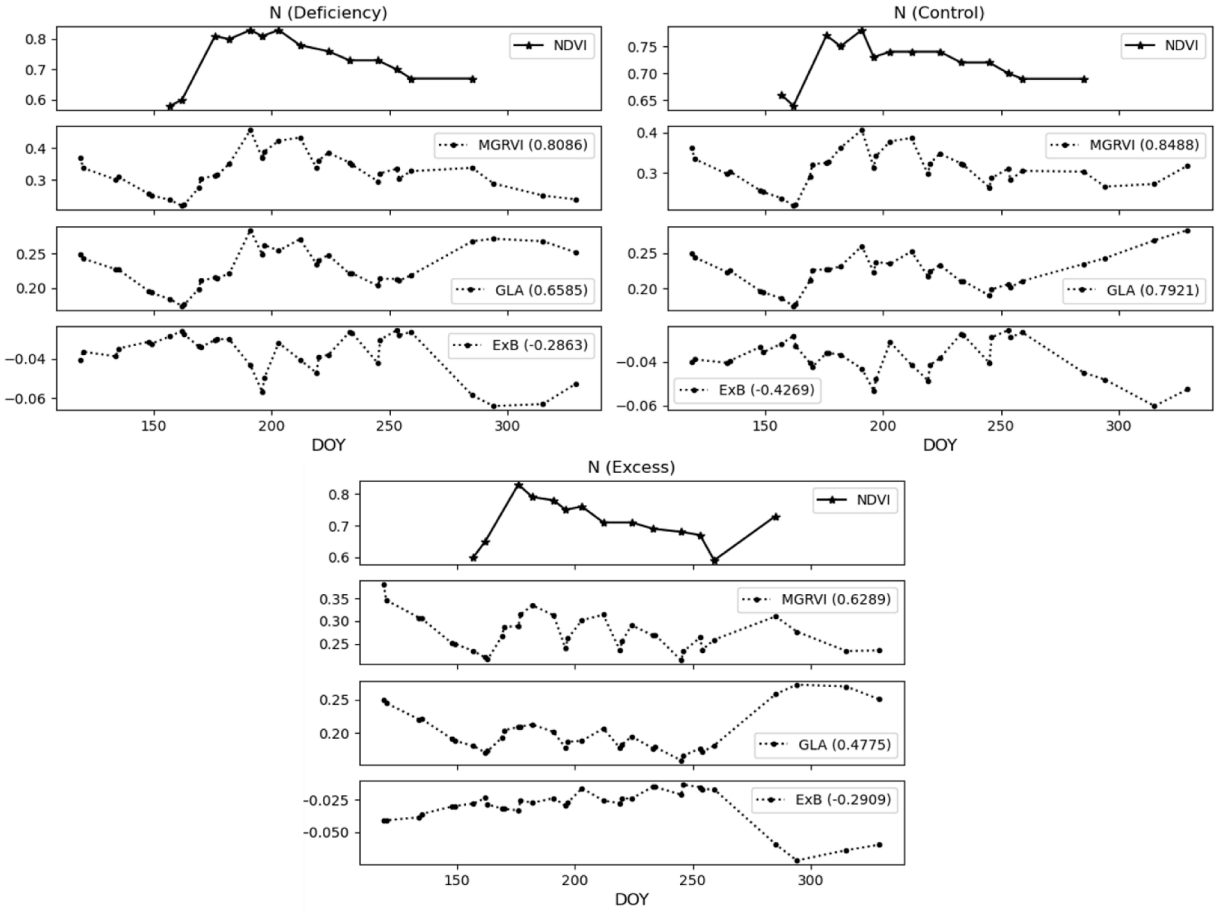

Fig. 6. Comparison of temporal evolution of NDVI, $MDVI^{N}_{MGRVI}$, $MDVI^{N}_{GLA}$, and $MDVI^{N}_{ExB}$ for trees under different nitrogen statuses.

capability in identifying extreme nutrient statuses. In contrast, the comparison between the deficiency and control groups resulted in lower values, indicating the difficulty in distinguishing nutrient deficiencies from the normal range. This finding poses a challenge in practical applications where the detection of deficiencies is of significant interest.

Notably, during the fruit production and harvest period (DOY 163 to DOY 259), the density distributions for the deficiency status in nitrogen and phosphorus groups shifted to higher values compared to the control and excess statuses. This observation can be explained by the heavy utilization of available nutrients in the crop during this period. Thus, the increased differentiation during this period further emphasizes the effectiveness of VIs in capturing nutrient variations.

The strong correlation between MGRVI for nitrogen group and NDVI supports the idea that MGRVI serves as a suitable indicator of vegetation health and biomass estimation. Bendig et al. (2015), which focuses on biomass prediction in a summer barley experiment, also highlights the potential of visible band vegetation indices, including MGRVI, for biomass estimation. This concurrence with a similar study reinforces the notion that MGRVI, along with other visible band indices, holds promise for various applications in vegetation monitoring and assessment.

Overall, our study aligns with the findings of Ge et al. (2021) and Qiu et al. (2021) by highlighting the importance of VIs derived from UAV-based RGB images in assessing macronutrient status. The correlation between MGRVI and nutrient status observed in our study reinforces the feasibility of using UAV-based remote sensing systems for cost-effective and efficient monitoring of crop growth traits and nutrient parameters.

6. Conclusion

We showed that a temporal analysis of VIs computed from aerial RGB images can be used to differentiate between macronutrient and water statuses for Hass avocado trees. Moreover, we proposed a comparison metric called MDVI that allows better differentiation among statuses for different groups and VIs. Over eleven VIs, MGRVI has been found to be the best on this purpose based on a comparison metric that measures the difference of temporal signals computed from the VIs. MGRVI better differentiates between statuses for nitrogen and phosphorus groups in a period of time that coincides with the fruit production and harvesting period of the Hass avocado trees. In addition, MGRVI shows a positive strong relationship with NDVI. Future research will explore the use of MGRVI in studies using only RGB images as variable to correlate with macronutrient and water status obtained from laboratory analysis.

CRediT authorship contribution statement

Itamar Salazar-Reque: Conceptualization, Methodology, Software, Formal analysis, Investigation, Data curation, Writing – original draft, Writing – review & editing, Visualization. **Daniel Arteaga:** Conceptualization, Methodology, Investigation, Data curation, Writing – original draft, Writing – review & editing, Visualization. **Fabiola Mendoza:** Conceptualization, Investigation, Data curation, Validation. **Maria Elena Rojas:** Conceptualization, Investigation, Resources, Supervision. **Jonell Soto:** Investigation, Resources, Supervision, Funding acquisition. **Samuel Huaman:** Conceptualization, Methodology, Resources, Supervision. **Guillermo Kemper:** Conceptualization, Investigation, Resources, Supervision, Project administration, Funding acquisition.

Declaration of Competing Interest

The authors declare that they have no known competing financial interests or personal relationships that could have appeared to influence the work reported in this paper.

Data availability

Data will be made available on request.

Acknowledgement

To the World Bank and "PROCIENCIA" (formerly FONDECYT), an initiative of CONCYTEC, for the funds allocated to the project under the contract N° 097-2018-FONDECYT-BM-IADT-AV.

References

Adan, M., Abdel-Rahman, E.M., Gachoki, S., Muriithi, B.W., Lattorff, H.M.G., Kerubo, V., Landmann, T., Mohamed, S.A., Tonnang, H.E., Dubois, T., 2021. Use of earth observation satellite data to guide the implementation of integrated pest and pollinator management (IPPM) technologies in an avocado production system. Remote Sens. Appl.: Soc. Environ. 23, 100566.

Ballesteros, R., Ortega, J.F., Hernandez, D., Moreno, M.A., 2018. Onion biomass monitoring using uav-based rgb imaging. Precis. Agric. 19, 840–857.

Barbedo, J.G.A., 2019. A review on the use of unmanned aerial vehicles and imaging sensors for monitoring and assessing plant stresses. Drones 3 (2), 40.

J. G. A. Barbedo, A new automatic method for disease symptom segmentation in digital photographs of plant leaves 147 (2) (2017) 349–364.

Bayomy, H.M., Alamri, E.S., Rozan, M.A., 2023. Effect of roasting hass avocado kernels on nutritional value and volatile compounds. Processes 11 (2), 377.

Bendig, J., Yu, K., Aasen, H., Bolten, A., Bennertz, S., Broscheit, J., Gnyp, M.L., Bareth, G., 2015. Combining UAV-based plant height from crop surface models, visible, and near infrared vegetation indices for biomass monitoring in barley. Int. J. Appl. Earth Obs. Geoinf. 39, 79–87.

Buschmann, C., Nagel, E., 1993. In vivo spectroscopy and internal optics of leaves as basis for remote sensing of vegetation. Int. J. Remote Sens. 14 (4), 711–722.

Chungcharoen, T., Donis-Gonzalez, I., Phetpan, K., Udompetaikul, V., Sirisomboon, P., Suwalak, R., 2022. Machine learning-based prediction of nutritional status in oil palm leaves using proximal multispectral images. Comput. Electron. Agric. 198, 107019.

Colombo, R., Papetti, A., 2019. Avocado (Persea americana mill.) by-products and their impact: from bioactive compounds to biomass energy and sorbent material for removing contaminants. a review. Int. J. Food Sci. Technol. 54 (4), 943–951.

Corrales-García, J.E., del Rosario García-Mateos, M., Martínez-López, E., Barrientos-Priego, A.F., Ybarra-Moncada, M.C., Ibarra-Estrada, E., Méndez-Zúñiga, S.M., Becerra-Morales, D., 2019. Anthocyanin and oil contents, fatty acids profiles and antioxidant activity of mexican landrace avocado fruits. Plant Foods Hum. Nutr. 74, 210–215.

Daughtry, C.S., Walthall, C., Kim, M., De Colstoun, E.B., Mc- Murtrey Iii, J., 2000. Estimating corn leaf chlorophyll concentration from leaf and canopy reflectance. Remote Sens. Environ. 74 (2), 229–239.

Dezordi, L.R., Aquino, L.A.d., Aquino, R.F.B.d.A., Clemente, J.M., Assunção, N.S., 2016. Diagnostic methods to assess the nutritional status of the carrot crop. Rev. Bras. Ciênc. Solo 40.

Gamon, J., Surfus, J., 1999. Assessing leaf pigment content and activity with a reflectometer. New Phytol. 143 (1), 105–117.

P. Gaona, L. Vásquez, C. Morales, W. Viera, P. Viteri, A. Sotomayor, L. Medina, P. Mejía, Y. Cartagena, Efecto de dos niveles de nitrogeno y potasio aplicados por fertirriego en las variables de crecimiento y concentración de macro y micronutrientes en plantas de aguacate (persea americana mill.) var. hass, in: ECUADOR ES CALIDAD, Vol. 7, 2020, 315 pp. 41–48. https://doi.org/10.36331/revista.v7i2.114.

Garza, B.N., Ancona, V., Enciso, J., Perotto-Baldivieso, H.L., Kunta, M., Simpson, C., 2020. Quantifying citrus tree health using true color UAV images. Remote Sens. (Basel) 12 (1), 170.

Ge, H., Xiang, H., Ma, F., Li, Z., Qiu, Z., Tan, Z., Du, C., 2021. Estimating plant nitrogen concentration of rice through fusing vegetation indices and color moments derived from UAV-RGB images. Remote Sens. (Basel) 13 (9), 1620.

Gitelson, A.A., Kaufman, Y.J., Stark, R., Rundquist, D., 2002. Novel algorithms for remote estimation of vegetation fraction. Remote Sens. Environ. 80 (1), 76–87.

Gitelson, A.A., Gritz, Y., Merzlyak, M.N., 2003. Relationships between leaf chlorophyll content and spectral reflectance and algorithms for non-destructive chlorophyll assessment in higher plant leaves. J. Plant Physiol. 160 (3), 271–282.

Gitelson, A.A., Vi ̃na, A., Ciganda, V., Rundquist, D.C., Arkebauer, T.J., 2005. Remote estimation of canopy chlorophyll content in crops. Geophys. Res. Lett. 32 (8).

Gitelson, A.A., Keydan, G.P., Merzlyak, M.N., 2006. Three-band model for noninvasive estimation of chlorophyll, carotenoids, and anthocyanin contents in higher plant leaves. Geophys. Res. Lett. 33 (11).

Guerra-Hernández, J., Díaz-Varela, R.A., Ávarez-González, J.G., Rodríguez-González, P. M., 2021. Assessing a novel modelling approach with high resolution UAV imagery for monitoring health status in priority riparian forests. Forest Ecosystems 8 (1), 1–21.

Haboudane, D., Miller, J.R., Tremblay, N., Zarco-Tejada, P.J., Dextraze, L., 2002. Integrated narrow-band vegetation indices for prediction of crop chlorophyll content for application to precision agriculture. Remote Sens. Environ. 81 (2–3), 416–426.

Hunt Jr, E.R., Daughtry, C., Eitel, J.U., Long, D.S., 2011. Remote sensing leaf chlorophyll content using a visible band index. Agron. J. 103 (4), 1090–1099.

Incrocci, L., Massa, D., Pardossi, A., 2017. New trends in the fertigation management of irrigated vegetable crops. Horticulturae 3 (2), 37.

Janoušek, J., Jambor, V., Marcoň, P., Dohnal, P., Synková, H., Fiala, P., 2021. Using UAV-based photogrammetry to obtain correlation between the vegetation indices and chemical analysis of agricultural crops. Remote Sens. (Basel) 13 (10), 1878.

Jay, S., Gorretta, N., Morel, J., Maupas, F., Bendoula, R., Rabatel, G., Dutartre, D., Comar, A., Baret, F., 2017. Estimating leaf chlorophyll content in sugar beet canopies

using millimeter- to centimeter-scale reflectance imagery. Remote Sens. Environ. 198, 173–186.
Jiaying, M., Tingting, C., Jie, L., Weimeng, F., Baohua, F., Guangyan, L., Hubo, L., Juncai, L., Zhihai, W., Longxing, T., Guanfu, F., 2022. Functions of nitrogen, phosphorus and potassium in energy status and their influences on rice growth and development. Rice Sci. 29 (2), 166–178.
Kosińska, A., Karamać, M., Estrella, I., Hernández, T., Bartolomé, B., Dykes, G.A., 2012. Phenolic compound profiles and antioxidant capacity of persea americana mill - peels and seeds of two varieties. J. Agric. Food Chem. 60 (18), 4613–4619. PMID: 22494370.
Louhaichi, M., Borman, M.M., Johnson, D.E., 2001. Spatially located platform and aerial photography for documentation of grazing impacts on wheat. Geocarto Int. 16 (1), 65–70.
Lu, Q.-Y., Arteaga, J.R., Zhang, Q., Huerta, S., Go, V.L.W., Heber, D., 2005. Inhibition of prostate cancer cell growth by an avocado extract: role of lipid-soluble bioactive substances. J. Nutr. Biochem. 16 (1), 23–30.
Lu, N., Wang, W., Zhang, Q., Li, D., Yao, X., Tian, Y., Zhu, Y., Cao, W., Baret, F., Liu, S., et al., 2019. Estimation of nitrogen nutrition status in winter wheat from unmanned aerial vehicle based multi-angular multispectral imagery. Front. Plant Sci. 10, 1601.
Mao, W., Wang, Y., Wang, Y., 2003. Real-time detection of between-row weeds using machine vision. In: 2003 ASAE Annual MeetIng. American Society of Agricultural and Biological Engineer, p. 1.
Megat Mohamed Nazir, M.N., Terhem, R., Norhisham, A.R., Mohd Razali, S., Meder, R., 2021. Early monitoring of health status of plantation-grown eucalyptus pellita at large spatial scale via visible spectrum imaging of canopy foliage using unmanned aerial vehicles. Forests 12 (10), 1393.
Meyer, G., Mehta, T., Kocher, M., Mortensen, D., Samal, A., 1998. Textural imaging and discriminant analysis for distinguishingweeds for spot spraying. Trans. ASAE 41 (4), 1189–1197.
Meyer, G.E., Neto, J.C., 2008. Verification of color vegetation indices for automated crop imaging applications. Comput. Electron. Agric. 63 (2), 282–293.
Noguera, M., Aquino, A., Ponce, J.M., Cordeiro, A., Silvestre, J., Arias-Calderón, R., da Encarnação Marcelo, M., Jordão, P., Andújar, J.M., 2021. Nutritional status assessment of olive crops by means of the analysis and modelling of multispectral images taken with UAVs. Biosyst. Eng. 211, 1–18.
Nyakang'i, C.O., Ebere, R., Marete, E., Arimi, J.M., 2023. Avocado production in kenya in relation to the world, avocado by-products (seeds and peels) functionality and utilization in food products. Appl. Food Res., 100275
Ong, E.S., Low, J., Tan, J.C.W., Foo, S.Y., Leo, C.H., 2022. Valorization of avocado seeds with antioxidant capacity using pressurized hot water extraction. Sci. Rep. 12 (1), 13036.
Osco, L.P., Junior, J.M., Ramos, A.P.M., Furuya, D.E.G., Santana, D.C., Teodoro, L.P.R., Gonçalves, W.N., Baio, F.H.R., Pistori, H., C. A. d. S. Junior,, et al., 2020. Leaf nitrogen concentration and plant height prediction for maize using UAV-based multispectral imagery and machine learning techniques. Remote Sens. (Basel) 12 (19), 3237.
Otsu, N., 1979. A threshold selection method from gray-level histograms. IEEE Trans. Syst. Man Cybern. 9 (1), 62–66.
Plett, D.C., Ranathunge, K., Melino, V.J., Kuya, N., Uga, Y., Kronzucker, H.J., 2020. The intersection of nitrogen nutrition and water use in plants: new paths toward improved crop productivity. J. Exp. Bot. 71 (15), 4452–4468.
Prado Osco, L., Marques Ramos, A.P., Roberto Pereira, D., Akemi Saito Moriya, É., Nobuhiro Imai, N., Takashi Matsubara, E., Estrabis, N., de Souza, M., Marcato Junior, J., Gonçalves, W.N., et al., 2019. Predicting canopy nitrogen content in citrus-trees using random forest algorithm associated to spectral vegetation indices from UAV-imagery. Remote Sens. (Basel) 11 (24), 2925.
Qiu, Z., Ma, F., Li, Z., Xu, X., Ge, H., Du, C., 2021. Estimation of nitrogen nutrition index in rice from UAV RGB images coupled with machine learning algorithms. Comput. Electron. Agric. 189, 106421 https://doi.org/10.1016/j.compag.2021.106421.
Robson, A., Rahman, M.M., Muir, J., 2017. Using worldview satellite imagery to map yield in avocado (persea americana): A case study in bundaberg, australia. Remote Sens. (Basel) 9 (12), 1223.
Ronneberger, O., Fischer, P., Brox, T., 2015. U-net: Convolutional networks for biomedical image segmentation. In: Navab, N., Hornegger, J., Wells, W.M., Frangi, A.F. (Eds.), Medical Image Computing and Computer-Assisted Intervention – MICCAI 2015. Springer International Publishing, Cham, pp. 234–241.
Roper, J.M., Garcia, J.F., Tsutsui, H., 2021. Emerging technologies for monitoring plant health in vivo. ACS Omega 6 (8), 5101–5107.
Rouse, J.W., Haas, R.H., Schell, J.A., Deering, D.W., et al., 1974. Monitoring vegetation systems in the great plains with erts. NASA Spec. Publ 351 (1), 309.
Saavedra, J., Córdova, A., Navarro, R., Díaz-Calderón, P., Fuentealba, C., Astudillo-Castro, C., Toledo, L., Enrione, J., Galvez, L., 2017. Industrial avocado waste: Functional compounds preservation by convective drying process. J. Food Eng. 198, 81–90.
Salazar-Reque, I., Arteaga, D., Huaman, K.G., Huamán Bustamante, S., 2021. A CNN-based algorithm for selecting tree-of-interest images acquired by UAV. In: 2021 IEEE International Conference on Machine Learning and Applied Network Technologies (ICMLANT), pp. 1–6. https://doi.org/10.1109/ICMLANT53170.2021.9690556.
Salgadoe, A.S.A., Robson, A.J., Lamb, D.W., Dann, E.K., Searle, C., 2018. Quantifying the severity of phytophthora root rot disease in avocado trees using image analysis. Remote Sens. (Basel) 10 (2), 226.
Sharifi, A., 2020. Remotely sensed vegetation indices for crop nutrition mapping. J. Sci. Food Agric. 100 (14), 5191–5196.
Silber, A., Naor, A., Cohen, H., Bar-Noy, Y., Yechieli, N., Levi, M., Noy, M., Peres, M., Duari, D., Narkis, K., et al., 2018. Avocado fertilization: Matching the periodic demand for nutrients. Sci. Hortic. 241, 231–240.
Silber, A., Goldberg, T., Shapira, O., Hochberg, U., 2022. Nitrogen uptake and macronutrients distribution in mango (Mangifera indica L. cv. Keitt) trees. Plant Physiol. Biochem. 181, 23–32.
Sims, N.C., Culvenor, D., Newnham, G., Coops, N.C., Hopmans, P., 2013. Towards the operational use of satellite hyperspectral image data for mapping nutrient status and fertilizer requirements in australian plantation forests. IEEE J. Sel. Top. Appl. Earth Obs. Remote Sens. 6 (2), 320–328.
Tucker, C.J., 1979. Red and photographic infrared linear combinations for monitoring vegetation. Remote Sens. Environ. 8 (2), 127–150.
van Dijk, M., Morley, T., Rau, M.L., Saghai, Y., 2021. A meta-analysis of projected global food demand and population at risk of hunger for the period 2010–2050. Nature Food 2 (7), 494–501.
Wang, W., Bostic, T.R., Gu, L., 2010. Antioxidant capacities, procyanidins and pigments in avocados of different strains and cultivars. Food Chem. 122 (4), 1193–1198.
Woebbecke, D.M., Meyer, G.E., Von Bargen, K., Mortensen, D.A., 1995. Color indices for weed identification under various soil, residue, and lighting conditions. Trans. ASAE 38 (1), 259–269.
Yue, J., Feng, H., Jin, X., Yuan, H., Li, Z., Zhou, C., Yang, G., Tian, Q., 2018. A comparison of crop parameters estimation using images from uav-mounted snapshot hyperspectral sensor and high-definition digital camera. Remote Sens. (Basel) 10 (7), 1138.
Zha, H., Miao, Y., Wang, T., Li, Y., Sun, J.W., Feng, Z., Kusnierek, K., 2020. Improving unmanned aerial vehicle remote sensing-based rice nitrogen nutrition index prediction with machine learning. Remote Sens. (Basel) 12 (2), 215.
Zhang, Y., Su, Z., Shen, W., Jia, R., Luan, J., 2016. Remote monitoring of heading rice growing and nitrogen content based on UAV images. International Journal of Smart Home 10 (7), 103–114.